IOP Conf. Series: Materials Science and Engineering **24** (2011) 012015 doi:10.1088/1757-899X/24/1/012015

Effect of Ewald sphere curvature on the GISAXS analysis of capped Germanium nanodot samples in the soft X-ray region

Hiroshi Okuda[1], Kohki Takeshita[1], Masayuki Kato[1], Shojiro Ochiai[1], and Yoshinori Kitajima[2]

[1]Dept. Mater. Sci. Eng. Kyoto University Sakyo-ku Kyoto 606-8501 Japan.

[2]Photon Factory, High Energy Accerelator Organization, Tsukuba 305-0801 Japan.

okuda@materials.mbox.media.kyoto-u.ac.jp

Abstract. Use of soft X-rays (SX) for assessing three dimensional structures in thin films by grazing-incidence small-angle X-ray scattering (GI-SAXS) has been discussed with an example of Ge nanodot structures grown on (001) Si substrates and capped with Si. GISAXS patterns obtained by the measurements were compared with model calculations, and several characteristic differences between GISAXS in the SX and that in hard X-rays have been discussed. It was concluded that although the curvature of the Ewald sphere slightly affects the two-dimensional GISAXS profiles, a two dimensional detector can be still used at the photon energy of about 2 keV. On the other hand, such effect may become dominant when the size of the nanostructure becomes smaller and the photon energy decreases.

1. Introduction

Grazing Incidence Small-Angle Scattering at a wavelength in Soft X-ray region, SX-GISAS, is a new technique to examine nanostructures near the materials surface. Although many works, including review articles have been published [1]-[5] on grazing incidence small-angle X-ray or Neutron scattering (GISAXS/GISANS) measurements and analysis, use of soft X-rays is not popular yet[6]-[9]. One of the reasons might be the experimental difficulties that everything should be placed in vacuum, including samples and detectors, since soft matters, including wet substances are not easily handled in such a system. Another reason would be the fact that it is not yet clear how the other effects, such as diffuse scattering at the surface, interfaces, and other structural inhomogeneities, or optical properties in the SX region influence the analysis. In the present work, GISAXS results and related simulations are presented to show how the GISAXS profiles of well-defined Ge nanodot structures look in the SX region at the K absorption edge of Si, which is relatively high energy for soft X-ray.

Although the nanodot structures comprising of Si substrate, Ge nanodots, and a Si cap layer are simple binary systems and use of anomalous dispersion is not necessarily critical for detailed analysis, use of anomalous dispersion at the Si K absorption edge would be a good measure to evaluate the validity of the data analysis procedures and the simulation model used to explain the experiment, since Si / Ge system is much more stable than soft materials, for which use of anomalous effect in SX has more significance, yet which are not stable enough to be used as a standard samples to assess the validity of the procedures.

2. Experimental

The samples used in the present measurements have been grown by MBE [10]. One layer of Ge nanodots have been grown on a Si (001) substrate and capped with a Si layer. The GISAXS measurements have been performed at beam-line 11B of Photon Factory, High Energy Accelerator Organization, KEK, Tsukuba Japan. The bending-magnet beamline has been designed mainly for XAFS measurements in relatively hard SX regions. A GISAXS measurement at SX region requires that all the experimental components are connected without atmospheric part to avoid strong absorption by air. Figure 1 is a schematic illustration of the experiment at the beamline. The beam was monochromated by a pair of InSb crystals and then shaped by a set of slits. The incident photon energies were chosen as 1.83 and 1.77 keV. Since the wavelength is more than 4 times longer than the conventional hard-X-rays used for GISAXS, corresponding camera length is much shorter than conventional SAXS experiments. The lower bound of the photon energy used in the present measurements was limited by the monochromater. The real parts of the atomic scattering factor, f_1, for Si and Ge are shown in Fig. 2 as a function of photon energy. As shown in the figure, the contrast between the nanodots and cap layer increases at the photon energy close to the absorption edge. When the contrast of the scattering object has strong contribution in imaginary part, it affects not only the scattering profile but also the reflectivity curve [11], where the interpretation of the scattering profile is more complex. However, the imaginary part of the scattering factor does not change much between the two energies used in the present work, and therefore, the difference in the GISAXS profiles should be explained in terms of the change in the real part.

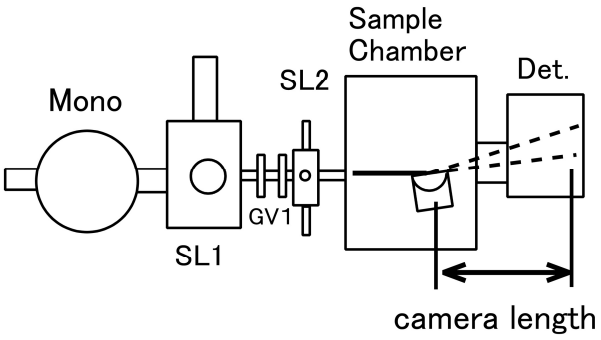

Figure 1. Schematic illustration of the GISAXS measurements at the beam-line 11B, Photon Factory. The camera length used in the present measurements was typically 400 mm.

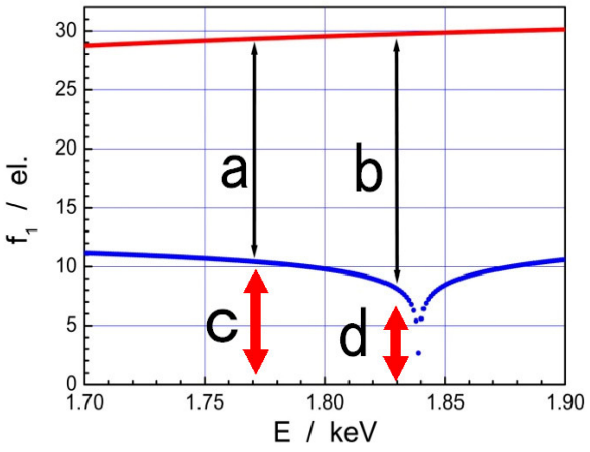

Figure 2. Real part of the atomic scattering factor for Si and Ge near the K absorption edge of Si. The change of the contrast between the cap layer and the vacuum is shown by red arrows, while that between the nanodots and the cap by black ones. Note that the GISAS intensity increases at the near-edge condition, while the surface scattering decreases.

The GISAXS patterns were obtained by using image plates with a standard SAXS method, i.e., with a fixed incident beam and two-dimensional simultaneous data acquisition. For the measurements with soft X-rays, the effect of the curvature of Ewald sphere may not be negligible. This effect has been evaluated by a set of simple calculations based on the pattern simulation of a model nanodot structures.

3. Results and Discussions

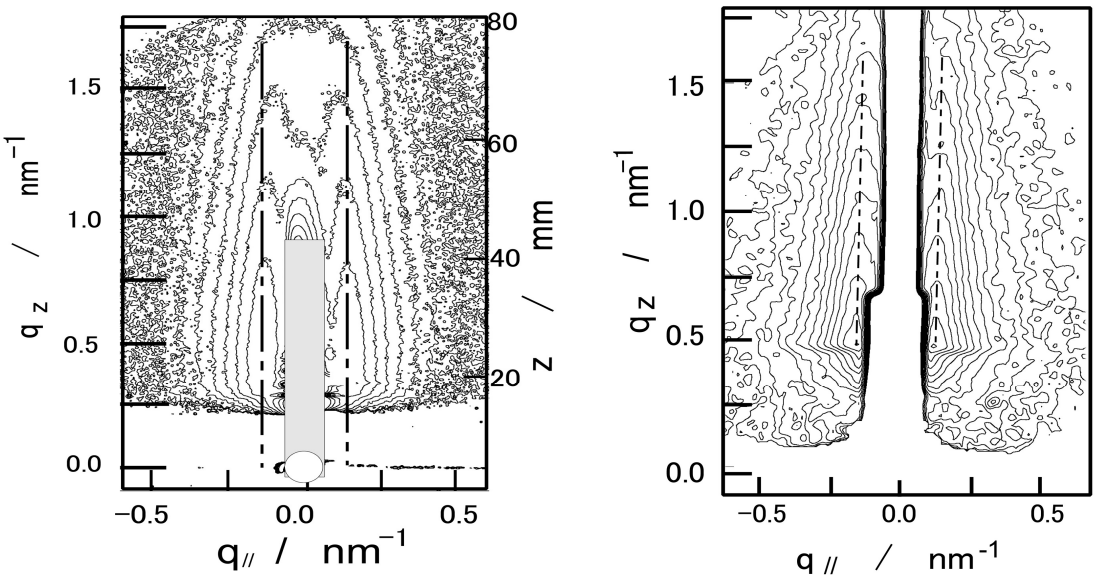

Figure 3. Two-dimensional contour of GISAXS intensity obtained at (a) 1.83 keV and (b) at 8.2 keV for the same Ge nanodot specimen. The position of Yoneda line is higher for 8.2 keV in q_z because of a shorter wavelength.

Two-dimensional GISAXS pattern obtained at the SX region of 1.83 keV (a) and that obtained at 8.2 keV are shown in Fig. 3. The contours are plotted in in-plane scattering vector, $q_{//}$, and out-of-plane scattering vector, q_z. The rectangular part around $q_{//}=0$ is a beam stop of direct beam and specular reflection. As discussed later, a fixed angle of incidence means that the data obtained in the out-of-plane direction do not agree with that for q_z because of the curvature of the Ewald sphere.

Use of soft X-rays for GISAXS measurements of the nanostructures has several merits and also drawbacks. Concerning the merits, 1. penetration depth is rather easily controlled with long wavelength, 2. anomalous dispersion effect for the lighter elements, such as Si, P, S becomes available, 3. low-q resolution is easily attained are attractive points for the measurements. On the other hand, A. measurements should be carried out in full vacuum due to strong absorption, B. curvature of Ewald sphere may not be negligible any more, are the drawbacks that can be readily recognized. The merit of controling penetration depth, i.e., depth-resolved GISAXS is an attractive one, and has been demonstrated for block copolymer films [12].

Comparing Fig 3 (a) with Fig. 3 (b), the patterns show similar tendency, i.e., monotonically decreasing intensity above the Yoneda line, with almost constant interparticle interference peak at 0.14 nm^{-1}. For further analysis of GISAXS intensity, the profile analysis using line cuts has been often used to assess the size of the scattering body, although it is not a gyration radius, etc., used in the standard SAS analysis in a rigorous sense and has been mainly used for parameter fitting in the intensity simulation[13],[14]. Blue broken/ dot lines in Figure 4 illustrate how the one-dimensional intensity profiles, i.e., 'line cuts', are taken in the present

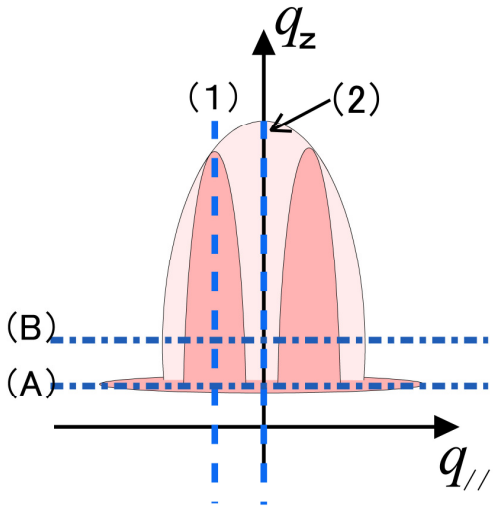

Figure 4. Schematic illustration of the position to extract line profiles (line cuts) from the present two-dimensional GISAXS patterns. In-plane line cut (B) and out-of-plane line cut (1) are used for the present analysis.

analysis. In the present analysis, the line cut in $q_{//}$ direction was taken slightly above the Yoneda line as shown by (B) to avoid unnecessary contribution of diffuse scattering at the surface. The vertical line cut in qz direction was taken at the peak intensity in $q_{//}$ direction, denoted as (1) in the figure, since the line cut denoted by (2) has difficulty both in measurement because of diffuse scattering by roughness and also in interpretation because of interparticle interference. From the Guinier analysis of in-plane line cuts, the in-plane gyration radius of 9.7 nm for SX almost agreed with that of 9.5 nm for 8.2 keV within experimental error [7]. The peak position in the in-plane direction, 0.14 nm^{-1}, also agreed each other, meaning that the interparticle distance of about 45 nm was obtained from both SX and hard-X-ray profiles. From the above results, it is concluded that the size parameters obtained for the present Ge nanodot from SX agreed with those obtained from hard X-ray reported before [10]. On the other hand, use of SX has a merit that contrast variation using Si K absorption edge is possible. In the present case, the system is binary, and therefore changing the contrast between nanodot and the cap layer is not essential for the nanostructure analysis. However, as discussed above, it is possible to examine the contribution of surface diffuse scattering to the total GISAXS intensity experimentally by using the anomalous effect, since the contrast between the vacuum and the Si surface is enhanced at the far-edge condition, while the contrast between the Si and Ge, which gives GISAXS intensity decreased at the far-edge condition. At the scattering vector larger than 0.1 nm^{-1}, the intensity ratio is almost constant, and the average was 1.35. It agreed with the expected change of the intensity calculated from the reported anomalous scattering factors [15]. In contrast, the intensity ratio at the smaller scattering vector decreased. It suggests that the recorded scattering intensity at small $q_{//}$ region comes mainly from the surface, i.e., roughness scattering at the sample surface whose contrast comes from the Si and vacuum, and decreases at the near edge condition. In principle, the contribution of diffuse scattering from the surface roughness can be separated experimentally by using this contrast change. In the present work, however it was not possible to separate the contribution of surface diffuse scattering, interface diffuse scattering and GISAXS since major part of the diffuse scattering was under the specular beam stop and also, because the measured GISAXS patterns had some indication that the scattering pattern in the low q// region might be modified by geometrical effect, namely, the curvature of Ewald sphere. However, it is concluded that the contribution of surface roughness scattering has been separated from the GISAXS.

Although the gyration radius obtained from hard X-ray and those obtained from SX GISAXS agreed each other, it is still necessary to examine the effect of wavelength on the structure parameters obtained from the measurement.

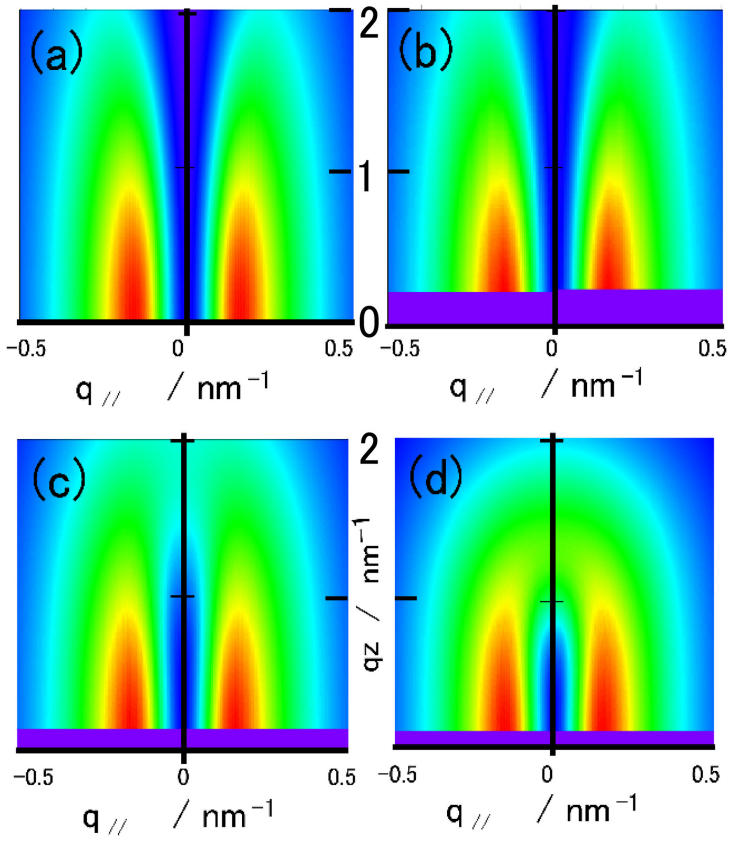

Figure 5. Simulated 2-dimensional intensity calculated for the structure parameters obtained from the present experimental data. Only the Born term is calculated for simplicity. (a) The intensity profile for the $q_{//}$-q_z plane, (b) projected for 0.15 nm, (c) 0.70 nm and (d) 1.55 nm of incident wavelength.

For this purpose, GISAXS profiles for the model nanodot systems with several wavelengths have been calculated using the parameters obtained from the present GISAXS measurements. Figure 5 gives the GISAXS patterns projected onto the detector plane (image plate in the present case). It simulates how the intensity distribution on a Ewald sphere with a fixed incidence angle is projected on an image plate. The calculation was made using only the Born term for simplicity, which has been proven to be a good approximation under some conditions [16]. Figure 5 (a) gives the model S(q) in the exact $q_{//}$-q_z reciprocal plane, and the profile agrees well with Fig. 5 (b), whose wavelength is 0.15 nm, close to that of Cu Kα radiation. However, at the present soft X-ray region of 0.7 nm, the interparticle interference appears different, i.e., the peaks shifted inward at high q_z region, which agrees with the experimental GISAXS pattern. This tendency becomes more apparent when the wavelength increased to 1.55 nm, corresponding to the energy close to the L edge of 3d metals. These changes in the GISAXS profiles are explained simply by taking the curvature of Ewald sphere into account. A simple geometric consideration gives that the scattering vector, q_z^0, where the two interparticle peaks of $q_{//}^m$ meet together is given by :

$$q_z^0 = \sqrt{(\frac{2\pi}{\lambda})^2 - (q_{//}^m - \frac{2\pi}{\lambda}\cos(\alpha_i))^2} + \frac{2\pi}{\lambda}\sin(\alpha_i) \qquad (1)$$

where λ, α_i are the wavelength of the incident photon and the incident angle, respectively. Equation 1 gives that q_z^0=1.74 nm^{-1} for λ=0.7 nm, and q_z^0=1.16 nm^{-1} for λ =1.55 nm. These results agree with the simulation in Fig. 5 and also the experimental pattern given in Fig. 3.

From the simulations above, it might be possible to estimate how the curvature of Ewald sphere affects the GISAXS analysis with a fixed angle of incidence. Figure 6 shows Guinier plot for the line

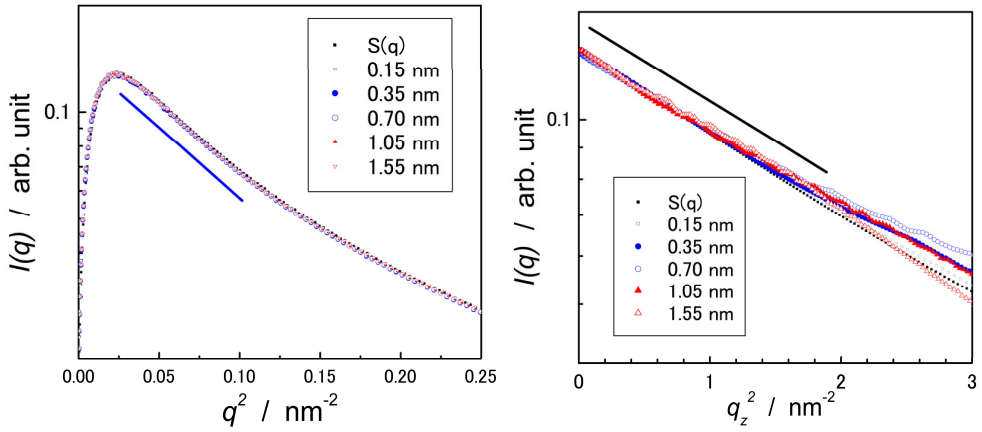

Figure 6. Simulated Guinier plots of the line cuts in $q_{//}$ (B) and q_z (1) directions calculated for several wavelengths. Straight lines are for the guide of the eye.

cuts in in-plane and out-of-plane directions of the two dimensional intensity profiles projected from Ewald sphere to the detector plane as shown in Fig. 5. It is noted that the plot is not the Guinier plot in the rigorous sense, since line cuts along $q_{//}$ is taken at a constant q_z, and that along q_z is taken at a constant $q_{//}$. Therefore, the plot may be justified when the shape of the dot is approximated such that the in-plane component and out-of-plane component of the form factor is independent, i.e., $S(q_{//},q_z)=S(q_{//})S(q_z)$ in a rigorous sense. However, the gyration radius obtained from the plot was found to give a good approximation by comparing the two dimensional intensity patterns. The position of line cuts are chosen as to be close to the condition used to analyze experimental GISAXS intensity, i.e., the $q_{//}$ line cuts were taken at q_z=0.5 nm^{-1}, and q_z line cuts at $q_{//}$=0.14 nm^{-1}, corresponding to the peak

position of interparticle interference for S(q). For the line cuts in $q_{//}$, the Guinier plots agreed well up to the very soft X-ray of 1.55 nm. Those in q_z direction agreed well in the small q regions. The apparent peak positions shift inwards because the two crossing points of isotropic interparticle interference peak with an Ewald sphere at each q_z eventually agree at a higher q_z for longer wavelength, meaning that the apparent interparticle distance increases for softer X-rays. Therefore, the apparent interparticle distance depends on the wavelength in principle. However, the plots in Fig. 6 suggest that the gyration radius is not affected by the curvature effect of the Ewald sphere in the present condition, even for much softer X-ray of about 0.8 keV.

It should be emphasized, however, that the present conclusions naturally depend on the relationship between the average size of the nanodots, i.e., the region of reciprocal space required for evaluation, and the wavelength used. In the present work, the average size of nanodots was about 20 nm in diameter and 4 nm in height, and 45 nm for nearest neighbour distance. If the size of the nanodot is one order of magnitude smaller, for example, then the region of interest in the reciprocal lattice becomes one order of magnitude larger. From the line cuts in Fig.6, it is easily expected that the scattering intensity may be strongly modified by the effect of the Ewald sphere curvature even in the Guinier region. Therefore, a model calculation becomes important to confirm the validity of analysis when the target structure is smaller and the incident photon energy becomes softer.

4. Conclusions

Grazing-incidence small-angle scattering measurements of Ge nanodots grown on a Si (001) substrate have been made at the Si K absorption edge. The effect of anomalous dispersion and that of the curvature of Ewald sphere on the analysis of the capped nanodot structure have been discussed with help of simple model calculations under Born approximation using the structure parameters obtained from the measurements. It is concluded that the effect of the curvature of the Ewald sphere gives impression of significant change of the overall shape of the scattering pattern for SX, when the measurements are made with standard GISAXS measurements of fixed incident angle. However, by choosing appropriate line cuts with a help of a model calculations, the effect becomes negligible. This is important since one of the most important merits of GISAXS is capability of real time measurements.

Part of the present work has been supported by Grant-in-aid for scientific research from JSPS, 22651034. The GISAXS experiment in the SX region has been performed under proposal #2009P002 and 2010G075 of Photon Factory, KEK Japan.

References

[1] Levine J.R. et al. 1989, J.Appl. Cryst. **22** 528.
[2] Naudon A., 1990, *Modern Aspect of Small-angle Scattering*, ed. H.Brumberger (Dordrecht: Kluwer) p181.
[3] Jin S. et al., 2007. J. Appl. Cryst., **40** 950..
[4] Renaud G., Lazzari R., and Leroy F., 2009. Surf. Sci. Rep. **64** 255.
[5] Yokoyama H. et al., 2007. J. Chem. Phys. **127** 014904.
[6] Stuhrman H.B. 2007. J.Appl. Cryst., **40** s23.
[7] Kotright J.B. et al., 2001. Phys. Rev. **B64** 092401.
[8] Okuda H., Kato M., Ochiai S. and Kitajima Y. 2010 Appl.Phys. Express, **2** 126501.
[9] Gutt C. et al., 2009. Phys. Rev. **B79** 212406.
[10] Okuda H. et al., 2002. Appl Phys. Letters **81** 2358.
[11] Ishiji K.et al.,2002. Phys. Rev. **B66** 014443.
[12] Okuda H. et al., 2011. J. Appl. Cryst. **44** No.2 *in press*
[13] Mueller-Buschbaum P. 2003. Anal. Bioanal. Chem. **376** 3.
[14] Salditt, T. et al., 1994 Phys. Rev. Lett. **73** 2228.
[15] http://physics.nist.gov/PhysRefData/FFast/html/form.html
[16] Okuda H. et al., 2010. J. Phys. Cond. Matter **22** 474003.